RSC Advances

ROYAL SOCIETY OF CHEMISTRY

www.rsc.org/advances

Graphical Abstract

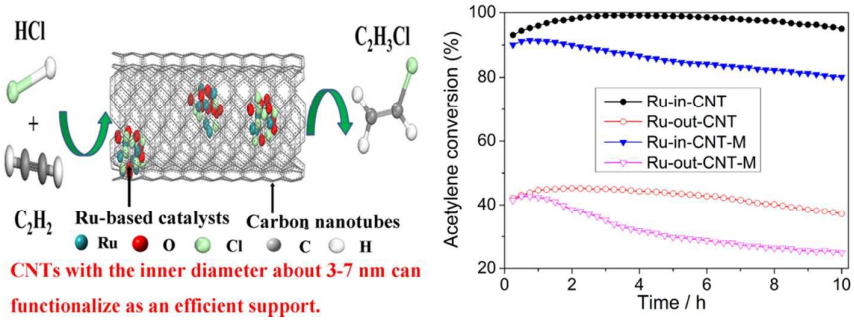

Highlights

• Ru catalysts deposited inside the channels of CNTs show higher catalytic activity.

• Ru-in-CNT catalyst exhibited the acetylene conversion of 95.0 % at 170 °C and 10 h.

• CNTs with the inner diameter of 3-7 nm can functionalize as an efficient support.

Non-mercury catalytic acetylene hydrochlorination over Ru catalysts enhanced by carbon nanotubes

Guangbi Li,[a,b] Wei Li[a], Haiyang Zhang[a], Yanfeng Pu[a], Mengxia Sun[a] and Jinli Zhang*[a]

[a] School of Chemical Engineering and Technology, Tianjin University, Tianjin 300072, P. R. China

[b] Department of Environmental Science and Engineering, Tianjin University of Science and Technology, Tianjin 300457, P. R. China

Dr. Jinli Zhang

Professor of Chemical Engineering

School of Chemical Engineering and Technology

Tianjin University, Tianjin 300072, China

TEL: +86-22-27890643

FAX: + 86-22-27890643

E-mail: zhangjinli@tju.edu.cn

Abstract

Ru-based catalysts with different deposition sites were prepared using multiwalled carbon nanotubes as the support and $RuCl_3$ as the precursor, in order to study the effects of multiwalled carbon nanotubes on the catalytic performance of Ru catalysts for acetylene hydrochlorination. It is suggested that Ru catalysts deposited inside the CNTs channels exhibit the optimal catalytic activity, with the acetylene conversion of 95.0 % and the selectivity to VCM of 99.9 % after 10 h on stream under the conditions of 170 °C and GHSV (C_2H_2) of 90 h^{-1}. In combination with characterizations of BET, TEM, XRD, TPR, TPD and XPS, it is illustrated that the CNTs with the inner diameter about 3-7 nm can functionalize as an efficient support with unique electron property to enhance the catalytic performance of Ru-based catalysts for acetylene hydrochlorination.

Keywords: acetylene hydrochlorination, ruthenium, carbon nanotubes, confinement

1. Introduction

Acetylene hydrochlorination reaction is an important coal-based industrial process to produce vinyl chloride monomer (VCM), which is the monomer to manufacture polyvinyl chloride via polymerization.[1] The reaction is carried out industrially using activated carbon-supported mercuric chloride as the catalyst,[2] which causes serious environmental pollution owing to high toxicity and volatility of the active mercuric chloride component. Thus, it is urgent to explore a reliable and environmental-benign non-mercury catalyst to substitute the poisonous mercuric chloride for acetylene hydrochlorination. Non-mercuric catalysts, involving the main metallic

component of Au,[3-5] Pd,[6,7] and Ru,[8-10] have been studied extensively, following the pioneer work of Hutchings.[11] However, it is still a challenge so far to develop an efficient non-mercury catalyst with high activity and long-term stability.

Multiwalled carbon nanotubes (CNTs) have a well-defined tubular structure formed by graphene layers with an electron-deficient interior surface and an electron-enriched exterior surface,[12-15] and are considered as the promising supports to adjust the activity of dispersed metal catalysts.[16-22] For examples, Bao and co-workers studied the effect of CNTs (with the inner and outer diameters about 4-8 and 10-20 nm, respectively) on the catalytic performance of Ru nanoparticles for ammonia synthesis reaction and reported that metallic Ru nanoparticles dispersed on the outside of CNTs displayed about two times higher turnover frequency than those dispersed inside the CNT channels.[23] Ran et al. studied the cellobiose conversion reaction over Ru nanoparticles and reported that the catalytic activity of Ru nanoparticles dispersed inside the CNT channels was higher than that dispersed on the outside of CNTs (with the inner and outer diameters about 3-6 and 10-20 nm, respectively).[24] It is suggested that the benificial deposition sites on CNTs for metallic catalysts are greatly associated with the distinct chemical reactions and the diameters of CNTs. Recently, Li et al. reported that polypyrrole-modified multiwalled carbon nanotubes (PPy-MWCNT) can enhance the catalytic activity of Au-based catatlysts for acetylene hydrochlorination.[25] These results enlightened us to study the effects of different Ru deposition sites of CNTs on acetylene hydrochlorination reaction.

In this article, we adopted multiwalled CNTs as the supports to prepare Ru-based catalysts deposited on the outside of CNTs or inside the channels of CNTs, and assessed the catalytic activity of these two kinds of Ru-based catalysts for acetylene hydrochlorination. In combination

with characterizations of BET, TEM, XRD, TPR, TPD and XPS, it is indicated that Ru-based catalysts deposited inside the channels of CNTs show greatly high catalytic activity for acetylene hydrochlorination.

2 Experimental

2.1 Materials

Analytical grade $RuCl_3 \cdot 3H_2O$ (the content of Ru assay 37.0 %) was purchased from Xi'an Kaida Chemical, Ltd. (China) and used without any purification. Two kinds of multiwalled CNTs (raw-CNT, raw-CNT-M) were purchased from Chengdu Organic Chemicals Co., LTD, China. The raw materials of multiwalled CNTs were treated by refluxing in concentrated HNO_3 (68.0 %) at 140 °C for 14 h, followed by filtration and washing in turn and then dessication at 60 °C for 12 h, in order to make the nanotube terminals open and the length of nanotubes cut into segments of 200-500 nm. The as-prepared CNTs were adopted as the supports to prepare Ru-based catalysts further. As shown in Fig. S1 of supplementary information, the support CNT has the inner and outer diameter of 3-7 nm and 8-15 nm respectively (denoted as CNT), while another support has the inner and outer diameter of 5-10 nm and 20-30 nm respectively (denoted as CNT-M).

2.2 Catalysts preparation

Adopting the support CNT, Ru-based catalysts deposited inside the channels of CNT (denoted as Ru-in-CNT) or on the outer surface of CNTs (denoted as Ru-out-CNT) were prepared using an improved wet chemistry method.[26-28] For the synthesis of Ru-in-CNT, the CNT (1.5 g) were dispersed in 70 mL solution of $RuCl_3$ in acetone by sonication for 6 h; the mixture was

continuously stirred at room temperature to allow slow evaporation of acetone, followed by a heated treatment in a tube furnace at 150 ℃ for 18 h with the air flow rate of 25 mL min^{-1}. For the synthesis of Ru-out-CNT, the CNT (1.5 g) were first dispersed in xylene solution (70 g) by ultrasonic treatment for 6 h so as to make the channels of CNT filled with xylene, then mixed with a $RuCl_3$ aqueous solution (2 mL) under magnetically stirring at 80 ℃. The obtained mixture was also treated in a tube furnace at 150 ℃ for 18 h with the air flow rate of 25 mL min^{-1}. In order to make the discussion clear in the next context, the blank support in-CNT was used to indicate the support CNT experienced the same treatment procedure to prepare Ru-in-CNT catalysts but without ruthenium trichloride precursors, while the blank support out-CNT was the support CNT experienced the same treatment to prepare Ru-out-CNT catalysts without ruthenium trichloride precursors.

In the case of another support CNT-M, we adopted the same procedures to prepare Ru-based catalysts deposited inside the channel of CNT-M (denoted as Ru-in-CNT-M) or on the outer surface of CNT-M (denoted as Ru-out-CNT-M). The Ru loading amount of all catalysts was 1 wt. % in this study, confirmed by the atomic absorption spectroscopy.

2.3 Catalyst characterization

N_2 adsorption/desorption experiments were conducted using a Quantachrome NOVA BET 2200e analyzer. The samples were first degassed at 300 ℃ for 4 h and analyzed via liquid nitrogen adsorption at -196 ℃. Transmission electron microscopy (TEM) was performed on a JEM 2100F field emission transmission electron microscope (JEOL, Tokyo, Japan) working at 200 kV using a scanning TEM mode (spot size, 0.4 nm). For sample preparation, the samples were first reduced in H_2 at 450 ℃ for 5 h and ultrasonically dispersed in ethanol, and then some

droplets of the suspension was dipped onto a holey carbon-coated copper grid and dried. X-ray powder diffraction (XRD) experiment was performed on a Bruker D8 Focus diffractometer using Cu Kα radiation at λ = 1.54056 Å with a scanning speed of 4 ° min^{-1} and a step of 0.02 ° (2θ) in the range from 20 ° to 80 °. X-ray photoelectron spectra (XPS) were obtained using a PHI 5000 Versa Probe (ULVAC-PHI Inc., Osaka, Japan) employing monochromatic Al Kα X-rays (hν = 1486.7 eV) under high vacuum condition. The data were collected at a sample tilt angle of 45 °. The binding energies were corrected using the C 1s peak of aliphatic carbon at 284.8 eV as an internal standard. The atomic absorption spectroscopy (AAS) was performed with a Perkin-Elmer 800 atomic absorption spectrometer using an air-acetylene flame. H_2 temperature programmed reduction (H_2-TPR) was performed on a TPDRO 1100 apparatus equipped with a thermal conductivity detector. For each test, 100 mg sample was heated from room temperature to 800 °C at a rate of 10 °C min^{-1}, flushing with a 20 mL min^{-1} gas mixture containing 5 % H_2 in N_2 gas. Temperature-programmed desorption (TPD) was analyzed by TPDRO 1100 apparatus. The samples were pretreated under hydrogen chloride and acetylene atmosphere at the reactive temperature (170 °C) for 6 h, respectively. Then high-purity N_2 (50 mL min^{-1}) was passed through the sample at 100 °C for 30 min. The TPD profiles were recorded for the sample heated from 100 °C to 650 °C with a rate of 10 °C min^{-1}.

2.4 Catalytic performance evaluation

The catalytic performance was investigated using a fixed-bed glass micro-reactor (i.d. of 8 mm). Acetylene (99.9% purity) was passed through silica-gel desiccant to remove trace impurities, and hydrogen chloride gas (99.9% purity) was dried using 5A molecular sieves. Acetylene (3 mL min^{-1}) and hydrogen chloride (3.3 mL min^{-1}) were introduced into a heated

reactor containing catalyst (2 mL) through a mixing vessel via calibrated mass flow controllers, giving a C_2H_2 gas hourly space velocity (GHSV) of 90 h^{-1} at 170 °C. This microreactor was purged with nitrogen before reaction to remove water and air. The reactor effluent was passed through an absorption bottle containing sodium hydroxide solution to remove unreacted hydrogen chloride. And then, the gas mixture was analyzed by Beifen GC-3420A gas chromatograph (GC).

3 Results and discussion

3.1 Catalyst characterization

3.1.1 Catalyst texture properties

BET measurements were performed to investigate the physical structure changes of CNT caused by the treatment of nitric acid, acetone, or xylene. Table 1 lists the specific surface area, pore volume and pore diameter of the raw material CNT, the CNT support treated by nitric acid, the blank in-CNT support experienced the same treatment procedure to prepare Ru-in-CNT catalysts but without ruthenium precursors, and the blank out-CNT support experienced the same treatment procedure to prepare Ru-out-CNT catalysts without ruthenium precursors, as well as the fresh catalysts of Ru-in-CNT and Ru-out-CNT. It is clear that the nitric acid treatment makes the specific surface area increased from 192 to 236 m^2 g^{-1}, the total pore volume increased from 0.28 to 0.32 cm^3 g^{-1}, and the pore diameter increased from 3.03 to 3.82 nm. It is indicated that further acetone or xylene treatment results in a little decrease of both surface area and pore volume, comparing in-CNT or out-CNT with CNT. The morphology changes of these different nanotubes are characterized by TEM images, as displayed in Fig. S2. After deposition of

ruthenium chloride, the surface area of the fresh catalyst Ru-in-CNT (220 m^2 g^{-1}) decreases by a fraction of 5 % comparing with in-CNT; while the pore volume of Ru-in-CNT (0.29 cm^3 g^{-1}) decreases by 3 % comparing with in-CNT, which is due to partial blocking of ruthenium species inside the support CNT. In the case of fresh catalyst Ru-out-CNT, both the surface area and the pore volume are similar with those of out-CNT.

Table 1 Pore structure parameters of different CNTs and the supported catalysts

catalyst	S_{BET} (m^2 g^{-1})	Pore volume (cm^3 g^{-1})	Pore diameter (nm)
raw-CNT [a]	192 ± 0.5[e]	0.28 ± 0.006	3.03 ± 0.006
CNT [b]	236 ± 0.8	0.32 ± 0.003	3.82 ± 0.006
in-CNT [c]	232 ± 0.8	0.30 ± 0.005	3.82 ± 0.002
out-CNT [d]	233 ± 0.5	0.31 ± 0.003	3.83 ± 0.003
Ru-out-CNT	232 ± 0.6	0.31 ± 0.005	3.81 ± 0.008
Ru-in-CNT	220 ± 0.8	0.29 ± 0.007	3.80 ± 0.007

[a]: The raw multiwalled CNTs purchased from Chengdu Organic Chemicals Co., LTD, China.

[b]: The CNTs treated by refluxing in concentrated nitric acid at 140 °C for 14 h, which are used as the support to prepare catalysts.

[c]: The blank in-CNT support, which is experienced the same treatment procedure to prepare Ru-in-CNT catalysts but without ruthenium trichloride precursors.

[d]: The blank out-CNT support, which is experienced the same treatment procedure to prepare Ru-out-CNT catalysts but without ruthenium trichloride precursors.

[e]: The data were obtained by the standard deviation.

3.1.2 Dispersion of Ru particles

Fig. 1 shows the XRD patterns of the support CNT, the fresh catalysts Ru-in-CNT and Ru-out-CNT. Apart from four characteristic diffraction peaks of CNT located at 25.6 ^{0}, 42.6 ^{0}, 53.1 ^{0} and 77.7 ^{0}, respectively,[29] neither of the fresh Ru-in-CNT and Ru-out-CNT shows peaks indicative of the hexagonal close-packed (hcp) metallic Ru phase or anhydrous tetragonal RuO_2, indicating that all Ru particles are very small (with the size lower than 4 nm),[30] which is in accord with TEM images (Fig. 2).

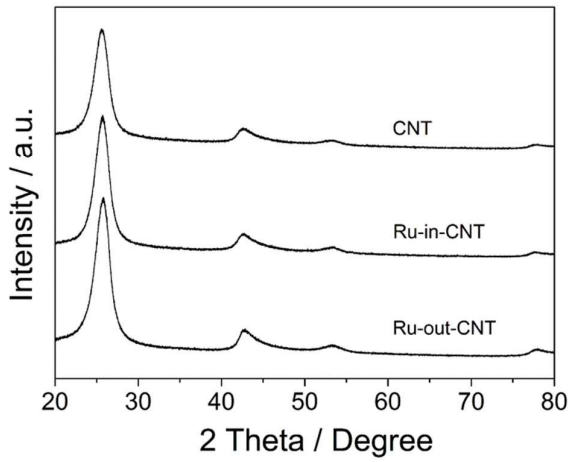

149

150 **Fig. 1** X-ray diffraction patterns of (a) the support CNT and the fresh catalysts (b) Ru-in-CNT and (c)
151 Ru-out-CNT.

152

153 Fig. 2 displays typical TEM images and the particle size distributions of the fresh catalysts
154 Ru-in-CNT and Ru-out-CNT reduced in H_2 at 450 °C for 5 h. For the fresh catalyst Ru-in-CNT,
155 Ru nanoparticles inside the channel of nanotubes have an average size about 0.95 nm, which is
156 smaller than the inner diameter of CNT (3-7 nm). The percentage of Ru nanoparticles deposited
157 inside the channel of CNT was calculated by counting the locations of 150-200 Ru particles on at
158 least 100 nanotubes. It is indicated that over eighty percent of ruthenium particles have been
159 introduced into the inner cavity of nanotubes (Fig. 2a). For the fresh catalyst Ru-out-CNT, Ru
160 nanoparticles are distributed exclusively on the exterior surface of CNT with the average size
161 about 1.01 nm (Fig. 2b).

162

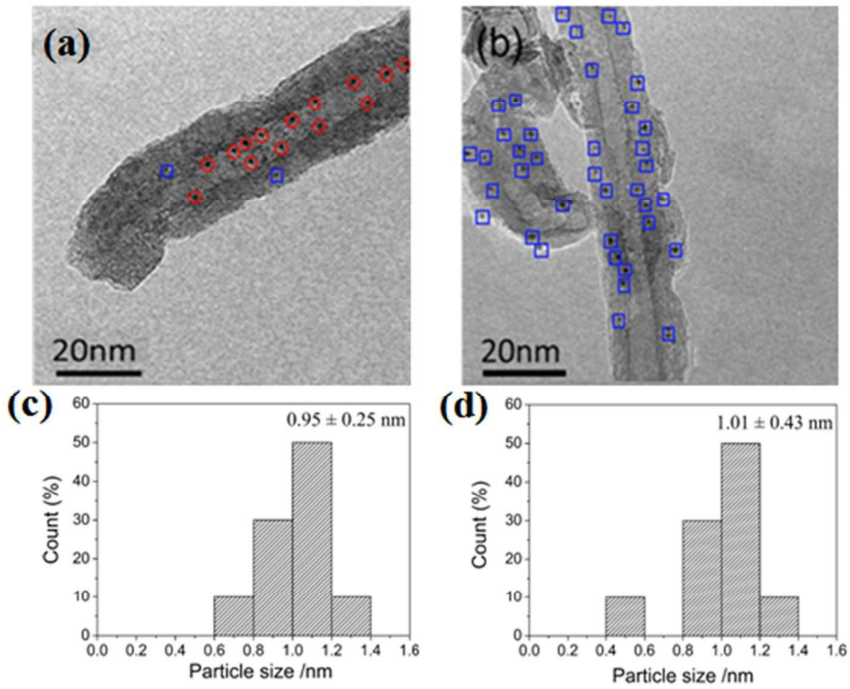

Fig. 2 TEM images and the particle size distributions of the fresh catalysts of Ru-in-CNT (a, c) and Ru-out-CNT (b, d). (Red circles: Ru nanoparticles confined within channels of CNT; blue squares: Ru nanoparticles located on external surfaces of CNT.)

3.1.3 Reducibility and adsorption property of Ru-based catalysts

H_2-TPR profiles were measured to evaluate the reducibility of two kinds of Ru-based catalysts using CNTs as the support. As shown in Fig. 3, TPR profiles of the fresh catalyst Ru-in-CNT and Ru-out-CNT are distinct from that of the blank support CNT. There are two broad peaks in the range of 350-800 °C for all the samples, which are attributed to the reduction of oxygenated groups in the CNT support.[23,31] There is a broad H_2 consumption peak in the temperature range of 100-350 °C for both Ru-in-CNT and Ru-out-CNT catalysts, compared with the profile of the support CNT, which is due to the reduction of ruthenium species involving the ruthenium oxides and ruthenium chloride in the catalysts.[23,32,33] It is noted that the reduction of ruthenium species takes place around 292 °C for Ru-in-CNT, whereas it occurs at a higher temperature (311 °C) for

Ru-out-CNT. It is known that the interaction between the electron-deficient concave surface of carbon nanotubes and the anionic chlorine in $RuCl_3$ or the anionic oxygen in RuO_2 could lead to weaken bonding strength of $RuCl_3$ or RuO_2 and consequently make it easier to reduce ruthenium species inside the channels of CNT. On the contrary, for Ru-out-CNT the weak interactions between the electron density-enriched outer surfaces of nanotubes with the anionic chlorine in $RuCl_3$ or the anionic oxygen in RuO_2, have less influence on the reducibility of ruthenium species.[15,23] Previous literatures also reported that ruthenium species inside CNT channel are easier to reduce compared to the outside ones.[23]

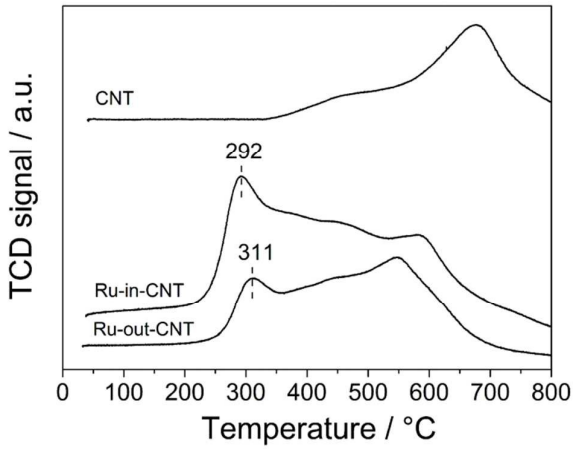

Fig. 3 H_2-TPR profiles of the support CNT (a), and the fresh catalysts of (b) Ru-in-CNT and (c) Ru-out-CNT.

TPD experiments were carried out to illustrate the adsorption property of the fresh catalysts Ru-in-CNT and Ru-out-CNT towards hydrogen chloride and acetylene. As shown in Fig. 4, the support CNT shows no obvious adsorption of hydrogen chloride, while the catalysts Ru-in-CNT and Ru-out-CNT show the obvious desorption peak of hydrogen chloride in the range of 205 ~ 295 °C, and the desorption area of hydrogen chloride from Ru-in-CNT is significantly larger

than that from Ru-out-CNT. For another reactant acetylene, as shown in Fig. 5, the catalysts Ru-in-CNT and Ru-out-CNT show the desorption peak of acetylene in the range of 190 ~ 430 °C, and the desorption area of acetylene from Ru-in-CNT is also larger than that from Ru-out-CNT. It is indicated that the catalyst Ru-in-CNT shows enhanced adsorption of both hydrogen chloride and acetylene, suggesting that the confinement within channels of CNT results in more active metallic sites in Ru-in-CNT and consequently promotes higher catalytic activities for the acetylene hydrochlorination reaction, as mentioned in the section 3.2.

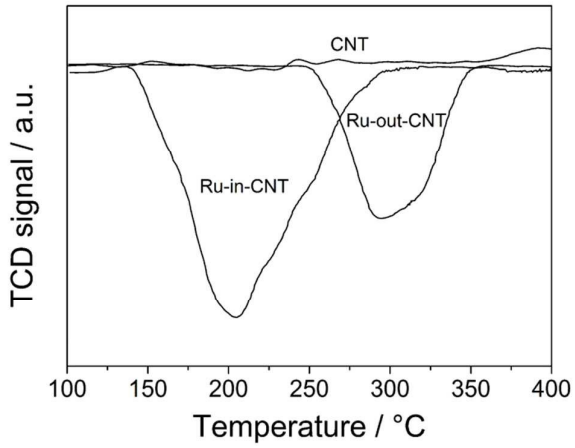

Fig. 4 HCl-TPD profiles of the support CNT (a), and the fresh catalysts of (b) Ru-in-CNT and (c) Ru-out-CNT.

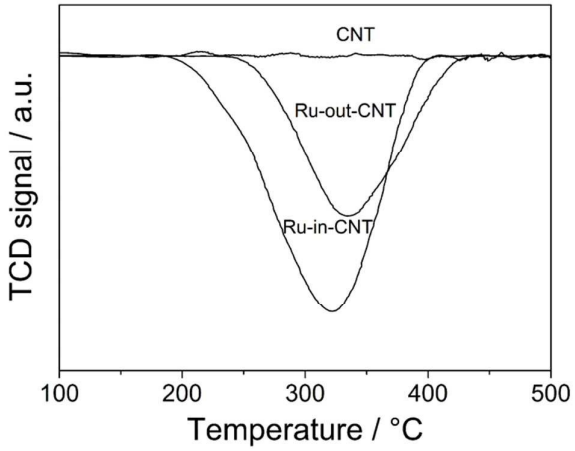

Fig. 5 C_2H_2-TPD profiles of the support CNT (a), and the fresh catalysts of (b) Ru-in-CNT and (c) Ru-out-CNT.

208

209 3.1.4 Ruthenium species associated with deposition sites on CNTs

210 Ru 3p3/2 XPS spectra of the fresh catalysts Ru-in-CNT and Ru-out-CNT were deconvoluted
211 into five peaks at 461.7 eV, 462.7 eV, 463.5 eV, 464.8 eV and 466.2 eV (Fig. S3), corresponding
212 to the species of metallic Ru, Ru/RuO_y, $RuCl_3$, RuO_2 and RuO_x, respectively.[34-37] The relative
213 content and binding energy of all the five Ru species are listed in Table 2. It is indicated that the
214 dominant species of Ru-in-CNT are RuO_2 (46.6 %) followed by Ru/RuO_y (24.4 %), RuO_x
215 (14.5 %), $RuCl_3$ (10.9 %) and metallic Ru (3.6 %), while the major species of Ru-out-CNT
216 include metallic Ru (28.1 %), RuO_2 (25.9 %) and $RuCl_3$ (24.5 %). It is well known that the
217 interior surface of CNT is electron-deficient whereas the exterior surface is
218 electron-enriched.[12,13,16] Thus, the ruthenium inside the channel of CNT works like the donor of
219 electrons so that the dominant species are high-valence oxidation states, while the ruthenium
220 deposited on the outer surface of CNT can easily accept electrons from CNT so as to generate
221 more amount of metallic Ru. It is illustrated that the deposition site of ruthenium precursor plays
222 an important role in affecting the distribution of valence states of ruthenium species in catalysts.

223

224 **Table 2** The binding energy (eV) and relative content (Area %) of ruthenium species in the fresh catalysts
225 Ru-in-CNT and Ru-out-CNT.

Catalysts	Ru^0 eV(Area %)	Ru/RuO_y eV(Area %)	$RuCl_3$ eV(Area %)	RuO_2 eV(Area %)	RuO_x eV(Area %)
Ru-in-CNT	461.7(3.6)	462.7(24.4)	463.5(10.9)	464.9(46.6)	466.2(14.5)
Ru-out-CNT	461.2(28.1)	462.3(13.0)	463.1(24.5)	464.8(25.9)	466.0(8.5)

226

227 **3.2 Catalytic performance for acetylene hydrochlorination**

The catalytic activity of different carbon nanotube supports was measured under the conditions of 170 °C and GHSV (C_2H_2) of 90 h^{-1}, and shown in Fig S4. It is indicated that the initial acetylene conversion is as low as 2.5 % over raw-CNT, CNT, in-CNT and out-CNT and decreases quickly. Fig. 6a and 6b show the catalytic performance of Ru-in-CNT and Ru-out-CNT for acetylene hydrochlorination. Over the catalyst Ru-out-CNT, the initial acetylene conversion is 45.2 % and decreases to 37.2 % after 10 h reaction. Whereas over Ru-in-CNT, the initial acetylene conversion is 99.1 % and decreases to 95.0 % after 10 h, and the selectivity to VCM maintains 99.9 %.

Adopting another carbon nanotube support CNT-M with the inner diameter of 5-10 nm, the catalytic performance of Ru-in-CNT-M and Ru-out-CNT-M is shown in Fig. 6c and 6d, under the same reaction conditions. Over Ru-out-CNT-M catalyst, the acetylene conversion decreases from 42.8 % to 24.9 % within 10 h reaction, whereas the selectivity to VCM increases somewhat from the initial 98.8 % to 99.8 % at 10 h. Over Ru-in-CNT-M catalyst, the acetylene conversion decreases from 91.4 % to 80.1 % within 10 h whereas the VCM selectivity maintains at 99.9 %.

In order to disclose the reason that the catalytic performance of Ru catalysts is dependent on the deposition sites of ruthenium precursors on the supports, TEM images and the particle size distributions of the fresh catalysts Ru-in-CNT-M and Ru-out-CNT-M were analyzed. As shown in Fig. S5, for the fresh catalyst Ru-in-CNT-M, Ru nanoparticles inside the channel of nanotubes have an average size about 1.66 nm. The percentage of Ru nanoparticles deposited inside the channel of CNT-M was calculated by counting the locations of 200 Ru particles on at least 100 nanotubes. It is indicated that over ninety percent of ruthenium particles have been introduced into the inner cavity of nanotubes. For the fresh catalyst Ru-out-CNT-M, Ru nanoparticles are

distributed exclusively on the exterior surface of CNT-M with the average size about 2.27 nm. Table S1 lists the surface area and the pore diameter of the support CNT-M and the supported Ru catalysts. After deposition of ruthenium precursors, the surface area of Ru-in-CNT-M decreases a little more than that of Ru-out-CNT-M, which is similar with those supported on CNT.

Further through the deconvolution of Ru 3p3/2 XPS spectra of the fresh catalysts Ru-in-CNT-M and Ru-out-CNT-M, the relative content and binding energy of Ru species are compared with those supported on CNT. As shown in Fig. S5, there are five peaks at 461.5 eV, 462.7 eV, 463.1 eV, 464.7 eV and 466.0 eV, due to the species of metallic Ru, Ru/RuO_y, $RuCl_3$, RuO_2 and RuO_x, respectively. The relative content and binding energy of all the five Ru species are listed in Table S2. It is indicated that the major species of Ru-in-CNT-M included RuO_2 (35.5 %), Ru/RuO_y (24.7 %), $RuCl_3$ (22.5 %), metallic Ru (14.3 %) and RuO_x (3.0 %), while the dominant species of Ru-out-CNT-M are $RuCl_3$ (70.1 %) followed by metallic Ru (13.7 %), RuO_2 (10.4 %), Ru/RuO_y (3.5 %) and RuO_x (2.3 %). It is indicated that RuO_2 is the most abundant species in both Ru-in-CNT and Ru-in-CNT-M. Previous work suggests that RuO_2 is the important active ingredient for the acetylene hydrochlorination.[10] Therefore, Ruthenium catalysts deposited in the channel of CNT with the inner diameter of 3-7 nm exhibit the optimal catalytic performance for acetylene hydrochlorination, which is associated with the abundance of RuO_2.

Previous literature reported that phenol, ether, and carbonyl groups on activated carbon surface are important to improve the catalytic activity of Au-based catalysts.[38] It is reasonable to consider that the carbon nanotubes experienced the treatment of nitric acid, acetone, or xylene possess different functional groups on the surfaces, which are probably associated with the catalytic performance of Ru-based catalysts. The effects of surface functional groups on

272 Ru-based catalysts will be studied in the future work.

273

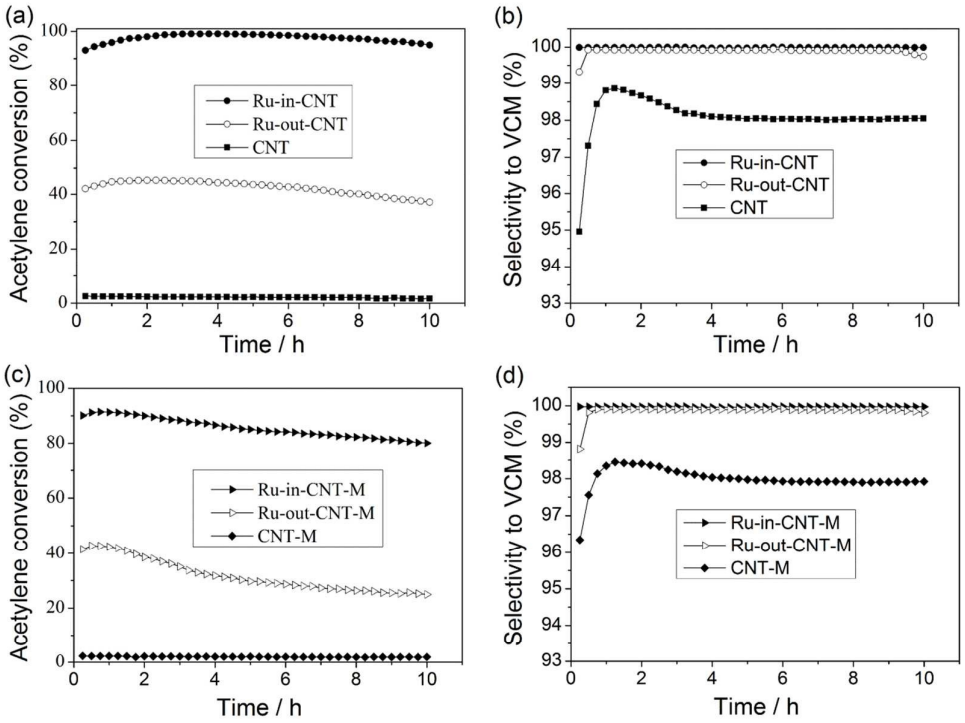

274

275 **Fig. 6** Catalytic performances of Ru-based catalysts deposited inside the channel of the support CNT (a, b) and
276 CNT-M (c, d), and those deposited in the outer surface of individual support. Reaction conditions: temperature
277 *(T)* =170 °C; C_2H_2 gas hourly space velocity (GHSV) = 90 h^{-1}; feed volume ratio $V_{HCl}/V_{C_2H_2}$= 1.1.

278

279 ## 4 Conclusions

280 Ru-based catalysts with different deposition sites were prepared using multiwalled carbon
281 nanotubes as the support and $RuCl_3$ as the precursor, in order to study the effects of multiwalled
282 carbon nanotubes on the catalytic performance of Ru catalysts for acetylene hydrochlorination.
283 Characterized by BET, TEM, XRD, TPR, TPD and XPS, it is suggested that Ru catalysts
284 deposited inside the CNTs channels exhibit the optimal catalytic activity, with the acetylene
285 conversion of 95.0 % and the selectivity to VCM of 99.9 % after 10 h on stream under the

conditions of 170 °C and GHSV (C_2H_2) of 90 h^{-1}. It is indicated that confinement inside CNTs can greatly influence the amount of ruthenium species involved in Ru^0, Ru/RuO_y, $RuCl_3$, RuO_2 and RuO_x in the preparation process of Ru-in-CNT catalyst, and enhance the adsorption of hydrogen chloride and acetylene over the catalyst. The acetylene conversion over these catalysts at 170 °C and 10 h decreases in the order of: Ru-in-CNT (95.0 %) > Ru-in-CNT-M (80.1 %) > Ru-out-CNT (37.2 %) > Ru-out-CNT-M (24.9 %). The excellent catalytic performance of Ru-in-CNT catalyst illustrates that the CNTs with the inner diameter about 3-7 nm can functionalize as an efficient support for Ru-based catalysts to enhance the acetylene hydrochlorination reaction.

Acknowledgements

This work was supported by the Special Funds for the Major State Research Program of China (No. 2012CB720302), the 863 Program (No. 2012AA062901), the NSFC (21176174), and the Program for Chang Jiang Scholars and Innovative Research Team in University (No. IRT1161).

References

1 N. Liu, J. Zhang, W. Li, B. Dai, Front. Chem. Sci. Eng., 2011, 5, 514-520.
2 J. B. Agnew and H. S. Shankar, Ind. Eng. Chem. Prod. Res. Dev., 1986, 25, 19-22.
3 M. Conte, C. J. Davies, D. J. Morgan, T. E. Davies, D. J. Elias, A. F. Carley, P. Johnston and G. J. Hutchings, J. Catal., 2013, 297, 128-136.
4 M. Conte, A. F. Carley, G. Attard, A. A. Herzing, C. J. Kiely and G. J. Hutchings, J. Catal., 2008, 257, 190-198.
5 H. Zhang, B. Dai, W. Li, X. Wang, J. Zhang, M. Zhu and J. Gu, J. Catal., 2014, 316, 141-148.
6 T. V. Krasnyakova, I. V. Zhikharev, R. S. Mitchenko, V. I. Burkhovetski, A. M. Korduban, T. V. Kryshchuk and S. A. Mitchenko, J. Catal., 2012, 288, 33-43.
7 S. A. Mitchenko, T. V. Krasnyakova and I. V. Zhikharev, Theor. Exp. Chem., 2010, 46, 32-38.
8 M. Zhu, L. Kang, Y. Su, S. Zhang and B. Dai, Can. J. Chem., 2013, 91, 120-125.
9 J. Zhang, W. Sheng, C. Guo and W. Li, RSC Adv., 2013, 3, 21062-21068.
10 Y. Pu, J. Zhang, L. Yu, Y. Jin, W. Li, Appl. Catal., A, 2014, 488, 28-36.
11 G. J. Hutchings, J. Catal., 1985, 96, 292-295.

12 R. C. Haddon, Science, 1993, 261, 1545-1550.
13 D. Ugarte, A. Châtelain and W. A. de Heer, Science, 1996, 274, 1897-1899.
14 B. Shan and K. Cho, Phys. Rev. B: Condens. Matter Mater. Phys., 2006, 73, 081401(R).
15 W. Chen, X. Pan, M. Willinger, D. Su and X. Bao, J. Am. Chem. Soc., 2006, 128, 3136-3137.
16 X. Pan, Z. Fan, W. Chen, Y. Ding, H. Luo and X. Bao, Nat. Mat., 2007, 6, 507-511.
17 W. Chen, Z. Fan, X. Pan and X. Bao, J. Am. Chem. Soc., 2008, 130, 9414-9419.
18 E. Castillejos, P. J. Debouttiere, L. Roiban, A. Solhy, V. Martinez, Y. Kihn, O. Ersen, K. Philippot, B. Chaudret and P. Serp, Angew. Chem., Int. Ed., 2009, 48, 2529-2533.
19 Z. Chen, Z. Guan, M. Li, Q. Yang and C. Li, Angew. Chem., Int. Ed., 2011, 50, 4913-4917.
20 Z. Guan, S. Lu and C. Li, J. Catal., 2014, 311, 1-5.
21 K. Zhou, J. Si, J. Jia, J. Huang, J. Zhou, G. Luo and F. Wei, RSC Adv., 2014, 4, 7766-7769.
22 L. Wang, J. Chen, L. Ge, V. Rudolph and Z. Zhu, RSC Adv., 2013, 3, 12641-12647.
23 S. Guo, X. Pan, H. Gao, Z. Yang, J. Zhao and X. Bao, Chem. - Eur. J., 2010, 16, 5379-5384.
24 M. Ran, Y. Liu, W. Chu and A. Borgna, Catal. Lett., 2013, 143, 1139-1144.
25 X. Li, M. Zhu, and B. Dai, Appl. Catal., B, 2014, 142-143, 234-240.
26 E. Dujardin, T. W. Ebbesen, H. Hiura and K. Tanigaki, Science, 1994, 265, 1850-1852.
27 S. C. Tsang, Y. Chen, P. J. F. Harris and M. L. H. Green, Nature, 1994, 372, 159-162.
28 C. Wang, S. Guo, X. Pan, W. Chen and X. Bao, J. Mater. Chem., 2008, 18, 5782-5786.
29 C. Jin, W. Xia, T. C. Nagaiah, J. Guo, X. Chen, M. Bron, W. Schuhmann and M. Muhler, Electrochim. Acta, 2009, 54, 7186-7193.
30 P. Gao, A. Wang, X. Wang and T. Zhang, Catal. Lett., 2008, 125, 289-295.
31 S. Kundu, Y. Wang, W. Xia and M. Muhler, J. Phys. Chem. C, 2008, 112, 16869-16878.
32 J. Kang, S. Zhang, Q. Zhang and Y. Wang, Angew. Chem., Int. Ed., 2009, 48, 2565-2568.
33 A. Guerrero-Ruiz, P. Badenes and I. Rodríguez-Ramos, Appl. Catal., A, 1998, 173, 313-321.
34 B. Folkesson, Acta Chem. Scand., 1973, 27, 287-302.
35 Y. Park, B. Lee, C. Kim, Y. Oh, S. Nam and B. Park, J. Mater. Res., 2009, 24, 2762-2766.
36 B. Yang, Q. Lu, Y. Wang, L. Zhuang, J. Lu, P. Liu, J. Wang and R. Wang, Chem. Mater., 2003, 15, 3552-3557.
37 A. B. Laursen, Y. Y. Gorbanev, F. Cavalca, P. Malacrida, A. Kleiman-Schwarsctein, S. Kegnæs, A. Riisager, I. Chorkendorff and S. Dahl, Appl. Catal., A, 2012, 433–434, 243-250.
38 J. Xu, J. Zhao, J. Xu, T. Zhang, X. Li, X. Di, J. Ni, J. Wang, and J. Cen, Ind. Eng. Chem. Res., 2014, 53, 14272–14281.